PNAS RESEARCH ARTICLE | BIOPHYSICS AND COMPUTATIONAL BIOLOGY
CHEMISTRY

A synergy between site-specific and transient interactions drives the phase separation of a disordered, low-complexity domain

Priyesh Mohanty[a,1], Jayakrishna Shenoy[b,1], Azamat Rizuan[a,1], José F. Mercado-Ortiz[b], Nicolas L. Fawzi[b,2], and Jeetain Mittal[a,c,d,2]

Edited by Pablo Debenedetti, Princeton University, Princeton, NJ; received April 6, 2023; accepted July 17, 2023

TAR DNA-binding protein 43 (TDP-43) is involved in key processes in RNA metabolism and is frequently implicated in many neurodegenerative diseases, including amyotrophic lateral sclerosis and frontotemporal dementia. The prion-like, disordered C-terminal domain (CTD) of TDP-43 is aggregation-prone, can undergo liquid-liquid phase separation (LLPS) in isolation, and is critical for phase separation (PS) of the full-length protein under physiological conditions. While a short conserved helical region (CR, spanning residues 319-341) promotes oligomerization and is essential for LLPS, aromatic residues in the flanking disordered regions (QN-rich, IDR1/2) are also found to play a critical role in PS and aggregation. Compared with other phase-separating proteins, TDP-43 CTD has a notably distinct sequence composition including many aliphatic residues such as methionine and leucine. Aliphatic residues were previously suggested to modulate the apparent viscosity of the resulting phases, but their direct contribution toward CTD phase separation has been relatively ignored. Using multiscale simulations coupled with in vitro saturation concentration (c_{sat}) measurements, we identified the importance of aromatic residues while also suggesting an essential role for aliphatic methionine residues in promoting single-chain compaction and LLPS. Surprisingly, NMR experiments showed that transient interactions involving phenylalanine and methionine residues in the disordered flanking regions can directly enhance site-specific, CR-mediated intermolecular association. Overall, our work highlights an underappreciated mode of biomolecular recognition, wherein both transient and site-specific hydrophobic interactions act synergistically to drive the oligomerization and phase separation of a disordered, low-complexity domain.

self-assembly | biomolecular recognition | phase separation

Significance

The RNA-binding protein TDP-43 is a component of neuronal inclusions associated with diseases such as amyotrophic lateral sclerosis, frontotemporal dementia, and Alzheimer's disease. The C-terminal domain (CTD) of TDP-43 is a disordered, low-complexity domain which is aggregation-prone and undergoes liquid–liquid phase separation (LLPS). CTD contains a hydrophobic, conserved region (CR, aa:319-341) which is α-helical and critical for oligomerization and LLPS. Using multiscale simulations and experiments, we report a noncanonical mechanism of biomolecular recognition wherein transient interactions involving hydrophobic residues in CR flanking regions drive the phase separation of CTD through direct enhancement of site-specific, CR-mediated interactions. Our study uncovers rich, mechanistic insights into CTD phase separation which is essential for understanding TDP-43 function and pathology.

Membraneless organelles, also referred to as biomolecular condensates, organize cellular biochemistry by sequestering functionally related macromolecular components from the bulk cellular environment (1–3). Experimental studies indicate that many of these organelles form via phase separation to create distinct subcompartments within either the nucleus or cytoplasm (4). These organelles include nucleoli, Cajal bodies, stress granules (SGs), and other ribonucleoprotein (RNP) granules (5). SGs, which primarily serve to sequester and halt the translation of mRNAs (6), recruit many distinct RNA-binding proteins (RBPs) and can form dynamically in response to physiological stress. In recent years, RBPs containing disordered, prion-like domains (e.g., FUS, hnRNPA2, hnRNPA1, TDP-43) have received considerable attention due to their involvement in SG assembly and maintenance (7). The prion-like, disordered regions (PrLDs) are typically enriched in polar residues (Ser, Thr, Asn, and Gln) and can undergo liquid–liquid phase separation (LLPS) in cells and as purified proteins in vitro via weak, multivalent interactions (8). Phase-separated droplets of prion-like domains can also mature to form fibril-like structures (9) which may exert a toxic cellular effect.

A constituent of SGs and other RNP granules that has received significant attention is TAR DNA-binding protein 43 (TDP-43), a primarily nuclear RBP that plays an essential role in the regulation of mRNA splicing (10). Mislocalization of TDP-43 to the cytoplasm due to chronic stress and/or in combination with mutations that disrupt its structure and interactions gives rise to the formation of ubiquitinated neuronal inclusions (11), a hallmark of amyotrophic lateral sclerosis (ALS). TDP-43 has a multidomain architecture consisting of an N-terminal folded domain that self-associates to form linear globular chains (12, 13), two RNA recognition motifs (RRMs) that together bind RNA (14), and a prion-like C-terminal domain (CTD) which is predominantly disordered (15, 16). Under in vitro conditions, the C-terminal domain readily phase separates in the presence of physiological concentrations of salt or RNA (16) which is enhanced at low temperatures (17). Within the CTD, there is an evolutionarily conserved, hydrophobic sequence that takes on an α-helical structure (15, 16) and is flanked by disordered regions—IDR1, Q/N, and IDR2 (*SI Appendix*, Fig. S1). Homooligomerization through this conserved region (CR) makes

Author contributions: P.M., N.L.F., and J.M. designed research; P.M., J.S., A.R., and J.F.M.-O. performed research; P.M., J.S., and A.R. analyzed data; and P.M., J.S., A.R., N.L.F., and J.M. wrote the paper.

The authors declare no competing interest.

This article is a PNAS Direct Submission.

[1]P.M., J.S., and A.R. contributed equally to this work.

[2]To whom correspondence may be addressed. Email: nicolas_fawzi@brown.edu or jeetain@tamu.edu.

This article contains supporting information online at https://www.pnas.org/lookup/suppl/doi:10.1073/pnas.2305625120/-/DCSupplemental.

Published August 14, 2023.

a large contribution to phase separation of the CTD; changes in helical stability through either ALS-related or designed mutations (16–19) were shown to tune phase separation. In addition to CR, aromatic residues in the flanking regions (IDR1/2) were also shown to be critical for LLPS (20, 21) and fibrillation of CTD (22).

A detailed bioinformatic analysis revealed the sequence conservation in IDR1/2 and the high conservation in the spacing of aromatic and hydrophobic residues (21). As shown in Fig. 1, TDP-43 CTD contains 8 phenylalanine (6 of them regularly spaced within the disordered flanking regions), 3 tryptophan, and 1 tyrosine. Both in vitro and in vivo experiments (17, 20, 21) point toward the essential nature of aromatic residues (F, W, Y) in driving the phase separation of TDP-43. While arginine-mediated interactions were found to be important for the condensate dynamics, neither electrostatics nor arginine-mediated interactions within the CTD were able to inhibit the LLPS of the TDP-43 reporter construct in vivo (21). While the importance of aromatic and charged residues in phase separation of TDP-43 CTD and other prion-like domains is well-established (23–26), the relative contributions of other residue types (e.g., aliphatic residues) to LLPS is less understood—previously viewed as playing a role in tuning the dynamics and solidification or aggregation but not in driving phase separation (21). Given the abundance of aliphatic hydrophobic residues within TDP-43 CTD—7 alanine, 5 methionine, and 2 leucine each in both the CR and the flanking disordered regions—their role in phase separation is important to define.

Significant advancements in the accuracy of enhanced sampling algorithms (27) and atomistic force fields (28, 29) allow for an in-depth characterization of the conformational landscape of intrinsically disordered proteins (IDPs) and regions (IDRs) (30–33), which complements insights obtained from biophysical experiments such as NMR, SAXS, and FRET (34, 35). Further, coarse-grained simulations parameterized based on amino acid hydrophobicity scales (36, 37) have provided valuable insights into the relationship between sequence and phase behavior of IDPs/IDRs. Here, we employed a multiscale simulation strategy based on atomistic and coarse-grained simulations coupled with in vitro phase separation experiments and NMR spectroscopy to probe the relative contributions of prevalent hydrophobic (phenylalanine and methionine) residues in CR and flanking regions on TDP-43 oligomerization and phase separation. Our results provide a detailed picture of TDP-43 CTD phase separation that helps to understand its function and pathology in the context of neurodegenerative diseases.

Results

Single-Chain Simulation Accurately Describes the Conformational Ensemble of TDP-43 C-Terminal Domain. The degree of compaction of disordered proteins at dilute concentrations positively correlates with their ability to undergo LLPS at higher concentrations (38, 39). Previously, we performed extensive characterization of small disordered fragments (<50 amino acids) belonging to RBPs such as LAF-1 (26), FUS (40), and hnRNPA2 (41) at the single-chain level. Because these phase-separating disordered domains contain repetitive sequence regions with low complexity, the analysis of intramolecular contacts observed in single-chain simulations mimicking the dispersed phase provided insights into intermolecular interactions implicated in phase separation. Exploiting this relationship, we first utilized enhanced sampling simulations to exhaustively sample and characterize at full atomic resolution, the diversity of interresidue interactions which drive TDP-43 CTD (aa: 267–414) conformational collapse at monomeric level. We utilized the AMBER99SBws-STQ protein force field with TIP4P/2005 water model, which provides an accurate description of the local and global

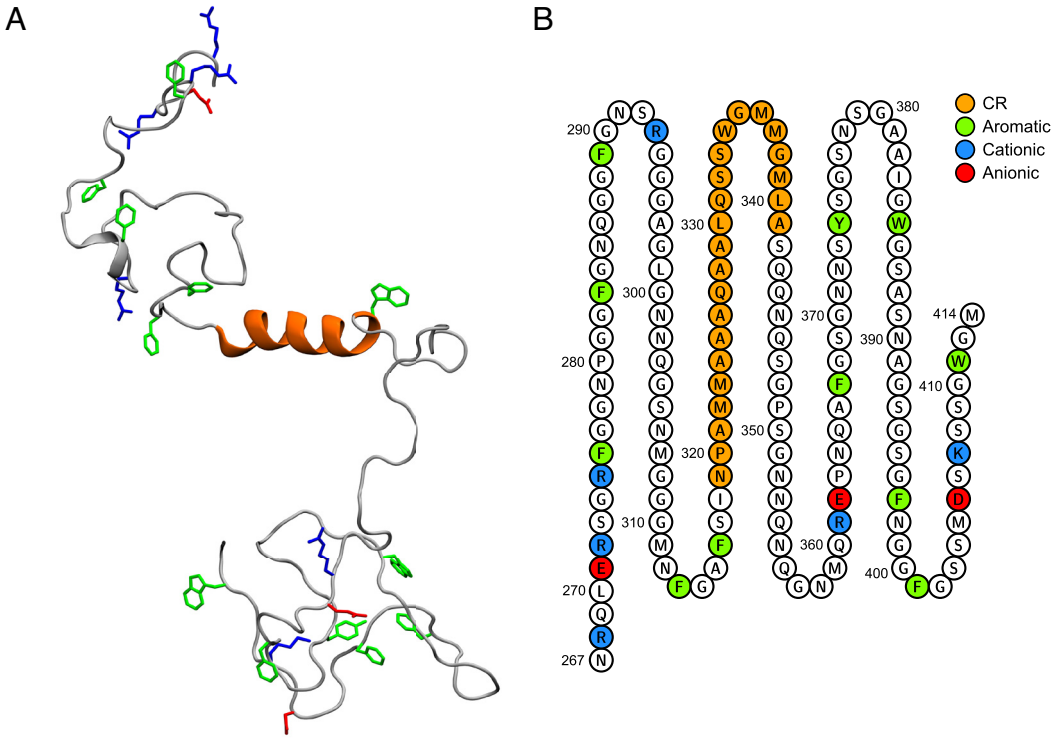

Fig. 1. Sequence composition of the TDP-43 CTD. (*A*) Cartoon representation of the C-terminal domain of TDP-43 that contains aromatic and charged residues outside the CR (spanning residue 319–341) enriched in aliphatic residues. (*B*) TDP-43 CTD (aa: 267–414) sequence. Letters in green, red, and blue circles are aromatic, anionic, and cationic residues, respectively. The residues within CR are shown as orange circles.

conformational properties of IDRs (42, 43). Despite the desired accuracy, a large computational cost is associated with adequate sampling of condensed-phase interactions and dynamics using atomistic MD simulations. Therefore, we utilized the residue-level contact information obtained from single-chain atomistic simulations to assess the accuracy of a coarse-grained model which uses a computationally efficient, single-bead-per-amino-acid representation to describe intra- and inter-molecular interactions within the condensed phase.

As TDP-43 contains a conserved helical region (aa: 319–341), it is important to ensure that the structural propensity of this region is accurately captured in the simulation. In our earlier studies (16, 19), single-chain simulations of the TDP-43 CTD fragment (aa: 310–350) performed using parallel tempering simulations in the well-tempered ensemble (PT-WTE) (44) faithfully captured the helical propensity of CR observed by NMR. Here, we performed PT-WTE simulations of the entire CTD (aa: 267–414) and first characterized its conformational properties. After establishing sufficient convergence (*Methods* and *SI Appendix*, Fig S2), the CTD ensemble at 300 K was compared to experimental NMR chemical shifts and secondary structure propensities (16). For the simulated ensemble, backbone $^{13}C_{\alpha}$ and $^{13}C_{\beta}$ chemical shifts, which provide residue-specific information on the secondary structure at each position, were predicted using the SPARTA+ algorithm (45). The root mean square deviation (RMSD) of chemical shifts with respect to experiment were less than 0.5 ppm which is within the prediction error and indicates good agreement (*SI Appendix*, Fig. S3*A*) similar to that for a subsegment of TDP-43 C-terminal domain (16). Per-residue secondary structure populations computed from simulation using DSSP (46) indicate helical propensity for residues in CR (*SI Appendix*, Fig. S4). The helical populations in the ensemble appear to be in reasonable agreement with those computed based on experiment chemical shifts using δ2D (47). δ2D predictions depend on the direct mapping of chemical shifts to secondary structure populations and utilize a training data set which contains both globular and disordered proteins. The accuracy of such predictors is, however, limited by the quality of the training dataset. A direct assessment of helical populations can be achieved by comparison of per-residue secondary chemical shift differences between simulation and experiment (Fig. 2*A* and *SI Appendix*, Fig. S3*B*). In agreement with experiment, positive values of the ^{13}C secondary shifts compared to those expected for a random coil reference ($\Delta\delta C_{\alpha}$ and $\Delta\delta C_{\alpha}$–$\Delta\delta C_{\beta}$ shifts) were observed for CR residues (aa: 320–330 and 335–342) which indicates the presence of α-helical structures (15, 16). In conclusion, PT-WTE simulations generated an accurate ensemble of CTD in terms of local conformational properties, which was suitable for the analysis of intramolecular interactions relevant to its phase separation.

Both Aromatic and Aliphatic Residues Contribute toward Single-Chain Compaction. To identify the critical residues that mediate TDP-43 CTD intramolecular interactions, we performed an in-depth analysis of pairwise residue contacts in the CTD ensemble generated by PT-WTE simulations. Two-dimensional contact maps of pairwise interactions based on residue index are shown in Fig. 2*B*. The interactions are classified into backbone–backbone (bb-bb), backbone–sidechain (bb-sc), and sidechain–sidechain (sc-sc) interaction modes. We find that residues within CTD contribute to the pairwise contacts via all three interaction modes, although sc-sc interactions are sparser owing to the abundance of glycine (~26%) in the CTD sequence which lacks a sidechain group. Next, position-specific interactions in CTD were also analyzed to identify residue positions that form a high number of contacts. To do so, we first derived the total number of per-residue contacts for each interaction mode through summation of all pairwise contacts at each residue position into a "one-dimensional" contact map (Fig. 2*C*). To assess the significance of each interaction mode, we also computed per-residue interaction energies (48) and analyzed their correlation with the corresponding number of contacts. A strong negative correlation was observed for bb-sc and sc-sc interactions, while bb-bb interactions showed a much weaker correlation (*SI Appendix*, Fig. S5). Hence, bb-sc and sc-sc interaction modes dominate the favorable energetic component of per-residue interactions in the single-chain ensemble. The total number of per-residue contacts summed over bb-sc and sc-sc interaction modes are shown in Fig. 2*C*.

Based on per-residue contact numbers, aromatic residues located outside the CR (F283/289/313/367, W385/412, and Y361) and R272/293 within IDR1 formed a high number of contacts (greater than mean+σ of $N_{contact}$ over all CTD residues) which is consistent with the established role of aromatic residues in driving phase separation of CTD (20) and the currently proposed, molecular grammar of the disordered prion-like domain phase separation (23, 25). Intriguingly, methionine residues (M307/311/336/337) within and outside of the CR also formed a high number of contacts. To examine the combined contribution of a particular residue type, we next calculated the total contacts formed by bb-sc and sc-sc atoms of all possible residue type pairs (*SI Appendix*, Fig. S6). As expected, the enrichment of glycine (G) and polar residues (S, N, and Q) in CTD results in an abundance of contact pairs that involve these residue types. As previously suggested, those residues may involve in variety of interaction modes such as backbone sp^2-π (49) and hydrogen bonding (40). However, other studies have suggested that these residue types may only play a minimal role in phase separation, only influencing the material properties of disordered prion-like domain condensates (23). As discussed above, we observed that aromatic (W and F) residues engage in a substantial number of interactions by their backbone and sidechain atoms. Consistent with observations from per-residue contact probabilities (Fig. 2*C*), methionines are among residues which formed a high number of contacts and were comparable in total to phenylalanines (*SI Appendix*, Fig. S6). Collectively, our contact analysis suggests that along with aromatic and polar residues, the presence of methionine residues may further increase the multivalency of CTD and contribute favorably toward its phase separation.

Coarse-Grained Simulations Predict the Importance of Nonalanine Aliphatic Residues in TDP-43 CTD Phase Separation. The observed intramolecular contacts in the single-chain ensemble from atomistic simulations may also contribute to the interchain interactions that stabilize the protein condensed phase (38). Therefore, the roles of key residues in CTD phase separation identified from the atomistic simulations can be further probed by performing phase coexistence simulations. Since AA simulations are computationally inefficient in studying the thermodynamic phase behavior, coarse-grained (CG) models that replace the atomistic details with a single-bead-per-amino-acid can be used to reach the time and length scales to study the phase separation of IDRs (36). For that reason, we conducted phase coexistence simulations of TDP-43 CTD using a recently developed CG model (37) based on the Urry hydrophobicity scale (50) (*Methods*). Because this CG model does not explicitly represent secondary structure propensity based on sequence, in these simulations, residues 320–341 were kept rigid in α-helical conformation using rigid body constraints (51) to partially mimic the structure identified by experiments and atomistic simulations. The qualitative behavior of TDP-43 CTD single-chain properties

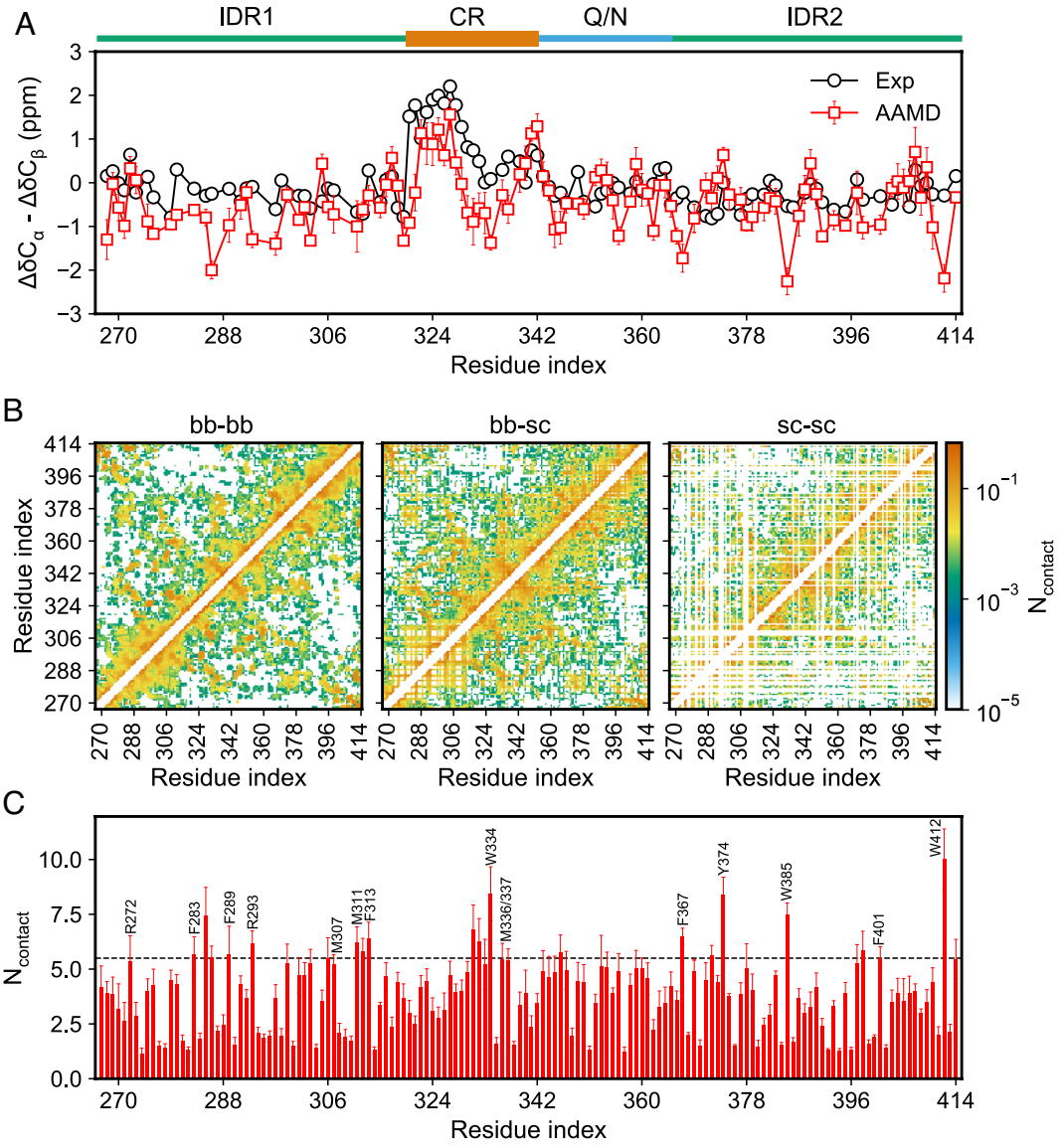

Fig. 2. Single-chain atomistic simulation of TDP-43 CTD highlight the contributions of aromatic and aliphatic residues toward chain compaction. (*A*) Validation of CTD ensemble at 300 K based on NMR-derived, per residue secondary chemical shift differences ($\Delta\delta C_\alpha$-$\Delta\delta C_\beta$). Secondary chemical shift differences from simulation show good overall agreement with the experiment. (*B*) 2D contact maps showing the average number of pairwise contacts ($N_{contact}$) over a 500 ns trajectory duration as a function of residue index, classified based on backbone–backbone (bb-bb), backbone–sidechain (bb-sc), and sidechain–sidechain (sc-sc) interaction modes. (*C*) Per-residue $N_{contact}$ plot derived via summation of over bb-sc + sc-sc contacts for each residue position based on 2D contact maps shown in *B*. Block averaging was performed over 100 ns intervals to obtain the mean and standard errors associated with each residue. The dashed line corresponds to the mean + σ cutoff used to identify individual residues which exhibit high $N_{contact}$ values. Analysis of intramolecular contacts suggests that multiple hydrophobic residues within and outside the CR may contribute toward CTD compaction.

from the CG simulations is consistent with the atomistic CTD ensemble at 300 K (*SI Appendix*, Fig. S7). Although single-chain CG simulations sample more extended CTD conformations, the number of residue-type contacts sampled from the CG simulations is in good agreement with the results of atomistic simulations described above (*SI Appendix*, Fig. S7). The mean value of R_g (3.05 ± 0.01 nm) from the single-chain CG simulations is also comparable to the approximate R_g of monomeric TDP-43 CTD (2.8 nm) based on its diffusion coefficient (19). These observations provide further confidence to use the CG model to study the CTD condensed phase. The slab geometry is utilized for CG simulations of phase coexistence that allowed efficient equilibration between the dilute and condensed phases (Fig. 3*A*). The intermolecular contact map of wild-type (WT) CTD (Fig. 3*B*) shows that each subdomain contributes to overall interactions to differing degrees, while self-interaction within the CR is slightly favored. Both per-residue and residue-type intermolecular contacts in the condensed phase were found to be in excellent agreement with intramolecular contacts from single-chain atomistic simulations (Fig. 3 *B* and *C* and *SI Appendix*, Fig. S8). These observations established a correspondence between single-chain and condensed-phase interactions and allowed us to test the ability of mutant CTD variants (Fig. 3 *A* and *D*) to form a stable condensed phase.

Given the highest abundance aromatic phenylalanine (8 in total) and aliphatic methionine (10 in total) residues, we first tested the impact of substitutions of these residue types on the stability of the condensed phase based on changes in the saturation concentration (c_{sat}) relative to WT CTD (Fig. 3*A*). To do so, we designed variants mutating these residues within and outside the CR independently (*SI Appendix*, Table S1). It is important to

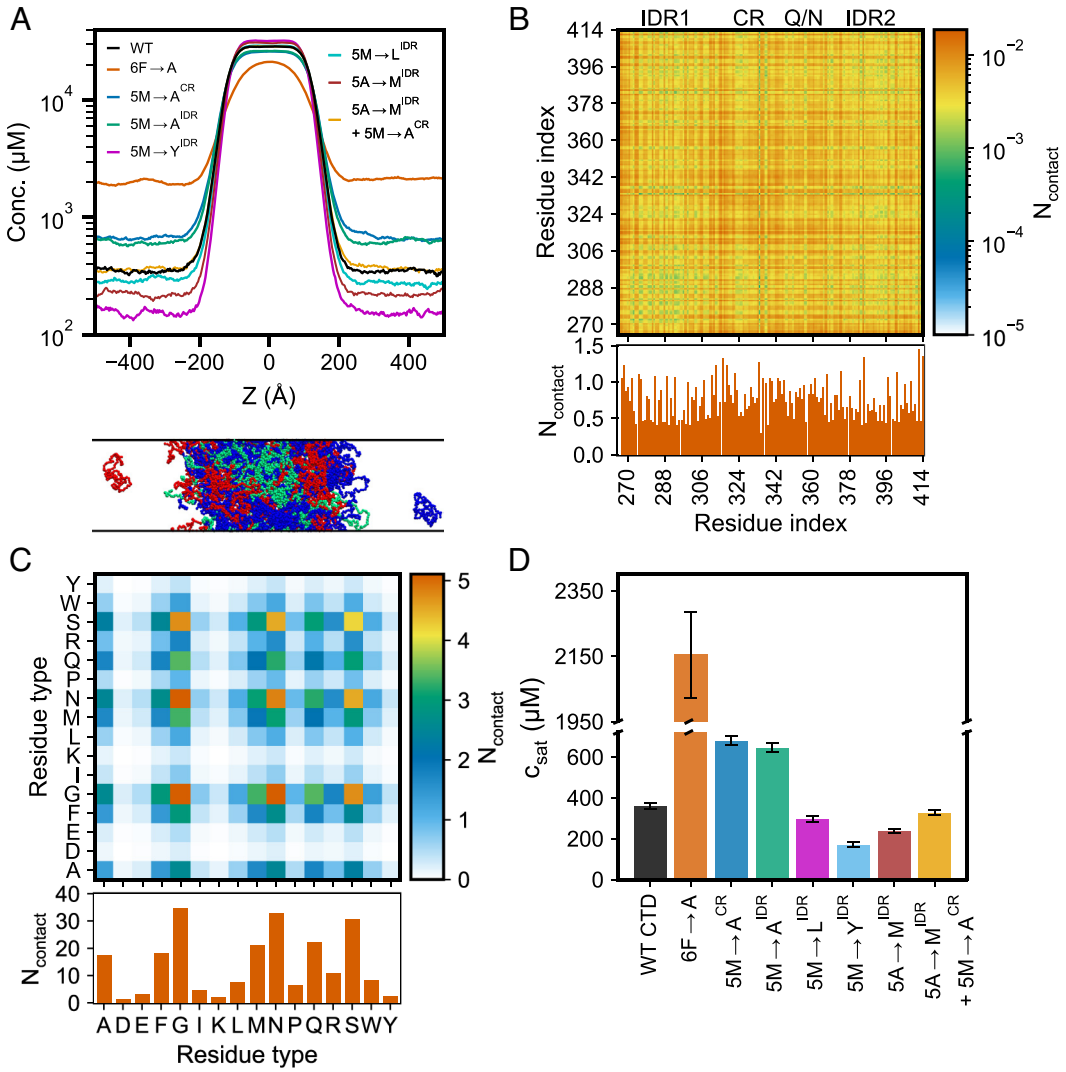

Fig. 3. CG phase coexistence simulations indicate the importance of aromatic and bulky aliphatic residues in phase behavior of TDP-43 CTD. (*A*) Snapshot of TDP-43 CTD WT slab configuration (100 chains) from CG simulation at 300 K, where two phases coexist (*Bottom*). The concentration profiles of TDP-43 CTD WT (black) and its variants along the z-dimension of the slab (*Top*). (*B*) Pairwise intermolecular interactions (*Top*) and number of contacts per residue (*Bottom*) in the condensed phase show the key residues involved in phase separation. (*C*) Pairwise interactions within the condensed phase as a function of residue type (*Top*) and its corresponding plot (*Bottom*) show the total number of contacts per residue type. (*D*) Saturation concentration (c_{sat}) for TDP-43 CTD WT and its variants computed based on concentration profiles in *A*.

mention that we carefully engineered these variants to avoid the disruption of helicity present in the CR, which is critical for CTD self-assembly. The aromatic mutant 6F→A (all phenylalanines to alanine, except F313, and F316, which are close to the CR) led to a >six-fold increase in $c_{sat,}$ indicating significant destabilization of the condensate. Next, the effects of methionine residues in the CR (5M→A^{CR}) and disordered flanking regions (5M→A^{IDR}) were tested by substituting them with alanine, keeping in mind that alanine has higher experimental helical propensity than methionine (52). Interestingly, mutational change in hydrophobicity by replacing methionine residues with alanine, both outside the CR (5M→A^{IDR}) and inside the CR (5M→A^{CR}), resulted in a lower phase separation propensity (~two-fold increase in c_{sat}) which indicates a favorable role for methionine residues in LLPS. Conversely, the substitution of methionines outside the CR with another aliphatic residue, leucine (5M→L^{IDR}), shows a similar c_{sat} as WT, hinting that the contribution to phase separation may not be specific to methionine but that other large aliphatic (nonalanine) residues could substitute. Meanwhile, mutating all five methionine residues outside the CR region to tyrosine (5M→Y^{IDR}) displayed substantial enhancement of phase separation (>two-fold decrease in c_{sat}). Thus, even if methionine (and leucine) are important contributors to phase separation, their relative contribution is lower than that of tyrosine, an aromatic residue which is found to be crucial for LLPS of many IDPs, including the low-complexity domains of FUS and hnRNPA1 (23, 25). Importantly, these variants shed light on the residue-level determinants of CTD phase separation, which may be universal to other phase-separating prion-like domains. Overall, the variation in c_{sat} observed for CTD mutants suggests that phenylalanines in the flanking disordered regions and methionine residues present within and outside the CR region significantly contribute to the phase separation of CTD.

Additional analysis of methionine residues via mutations using CG phase coexistence simulations suggests that methionines in both IDR1 (M307A and M311A) and IDR2 (M359A, M405A, and M414A) affect the phase behavior of CTD while substituting all methionine to alanine (10M→A) predicted to drastically weaken the phase separation compared to methionine variants examined above (*SI Appendix*, Fig. S9*A*). Positional mutational studies demonstrate that all individual methionine residues have

contributions toward LLPS and collectively stabilize the condensed phase of TDP-43 CTD (*SI Appendix*, Fig. S9*B*). These computational results further support the importance of methionine residues, which have not been previously recognized as essential for LLPS.

Phenylalanine and Methionine Residues Are Crucial for TDP-43 CTD Phase Separation In Vitro. To validate the observed trend in c_{sat} for WT CTD and its mutants observed in CG phase coexistence simulations, we tested the effect of these mutations on TDP-43 CTD phase separation in vitro by microscopy and droplet sedimentation assays (Fig. 4 and *Methods*). Droplet sedimentation assays provide a quantitative assessment of phase separation, wherein the concentration remaining in the supernatant after centrifugation of the suspended droplets provides a measure of the saturation concentration (c_{sat}) (53) for the WT and variants that do not undergo rapid conversion into static aggregates. Under the given buffer conditions, phase separation occurs if the protein concentration is equal to or above its c_{sat}.

WT CTD did not undergo phase separation in the absence of salt and showed an enhanced propensity for droplet formation upon increasing salt concentration (Fig. 4*A*), as shown previously (16, 19). In contrast, 6F→A mutation impaired droplet formation up to 120 μM protein concentration across all salt concentrations (Fig. 4*A*). Similarly, 5M→A^{CR} variant inhibits phase separation (c_{sat} > 120 μM). Hence, both mutants show much higher c_{sat} compared to WT (c_{sat} ~ 20 μM at 150 mM salt) (Fig. 4*B*). Notably, 5M→A^{IDR} variant exhibited phase separation at or above 75 mM NaCl, with nearly two-fold higher c_{sat} than WT, but much lower c_{sat} than 5M→A^{CR} (Fig. 4 *A*–*C*). Overall, the observed increase in c_{sat} for 6F→A and 5M→A^{IDR} mutants is consistent with predictions from CG simulations, showing that both of these residues are important for CTD phase separation, despite being outside the CR. However, it is important to note that the effects of methionine residues within the conserved helical region are substantially greater than those outside, suggesting the dramatic enhancement of phase separation via helix–helix contacts stabilized through methionine residues in the CR. We note that this difference between 5M→A^{CR} and 5M→A^{IDR} is not captured in the CG model results (Fig. 3*D*), which highlights directions for future improvements. This may involve adding an extra bead for distinguishing protein backbone versus sidechain to capture site-specific interactions within helical structures and sequence-specific changes in secondary structure and its modulation by oligomerization.

To test whether the importance of methionine residues generalizes to the alphabet of phase separation or only works for five evolutionarily conserved methionine positions within the flanking regions of CTD, 5 alanine residues within CTD flanks are mutated to methionine residues within the 5M→A^{CR} mutant (5A→M^{IDR} + 5M→A^{CR}), boosting the total methionine content in the flanking regions from 5 total to 10 total. Interestingly, the resulting mutant has a much lower c_{sat} than 5M→A^{CR} (~70 μM), showing that addition of methionine residues increases phase separation. DIC microscopy images confirm the formation of phase-separated droplets above 70 μM (*SI Appendix*, Fig. S10). However, in the context of wild-type CR, making the same

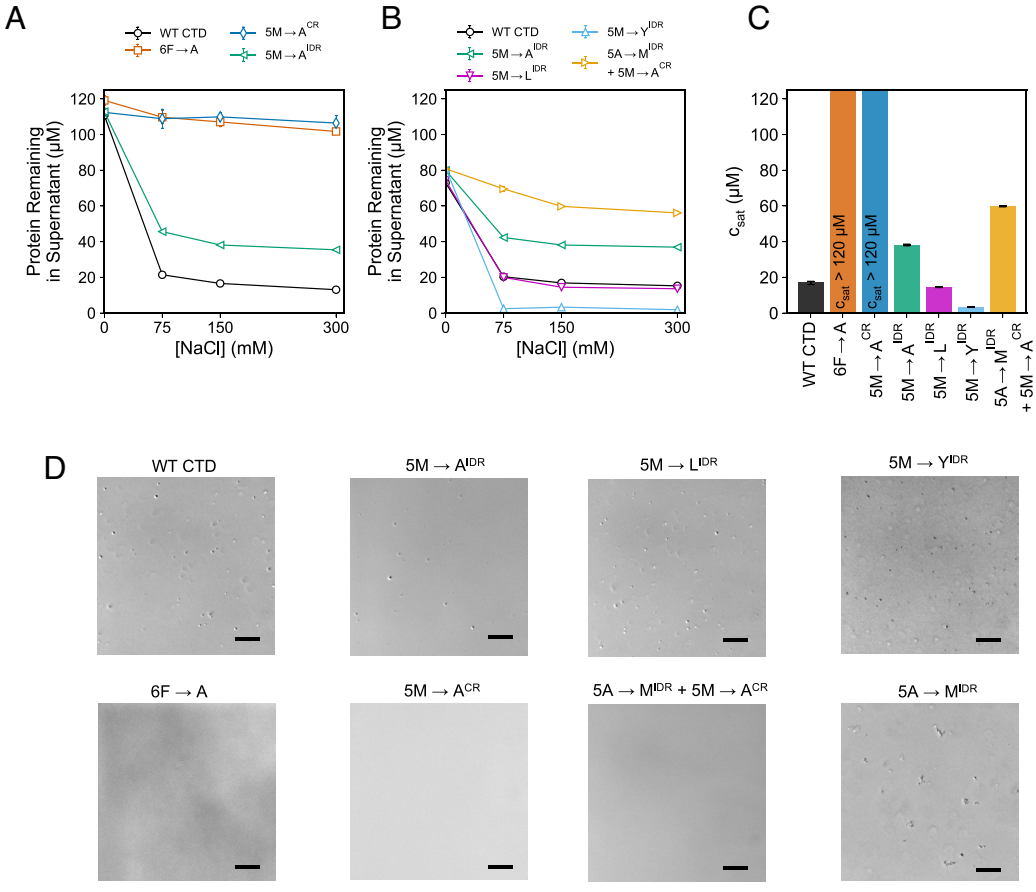

Fig. 4. Phenylalanine and methionine residues are crucial in TDP-43 CTD phase separation in vitro. (*A* and *B*) Quantification of phase separation assay showing the protein remaining in supernatant after phase separation for WT and its variants measured from 0 to 300 mM NaCl. Standard deviations of three replicates are represented as error bars. (*C*) Saturation concentration (c_{sat}) for TDP-43 CTD WT and its variants are determined by measuring supernatant concentration at 300 mM NaCl. (*D*) DIC micrographs for WT TDP-43 CTD (40 μM) and designed variants at 300 mM salt. (Scale bar, 20 μm.)

substitution of alanine to methionine (5A→M^{IDR}) results in the formation of non-moving round-shaped clusters at 150 mM NaCl and leads to irregularly shaped amorphous assemblies consistent with aggregation at 300 mM salt (Fig. 4*D* and *SI Appendix*, Fig. S11). Because this variant leads to rapid aggregation, we did not test the phase separation in the saturation concentration assay. The enhanced aggregation hints that the residues in the CTD sequence (especially methionine) are evolutionarily designed for an optimum number of occurrences. These two mutants further highlight the significance of methionine residues in modulating phase separation. A 5M→L^{IDR} mutant showed almost no change compared to WT, whereas 5M→Y^{IDR} lowered c_{sat} by an order of magnitude (Fig. 4 *A*–*C*). These results are consistent with the predictions from the CG simulations (Fig. 3 *D*), highlighting the importance of aliphatic residues for phase separation along with the aromatic residues.

Phenylalanine and Methionine Residues Are Important for CTD Self-Assembly. Finally, we evaluated the impact of these mutations inside and outside the CR that affect phase separation on the helical structure of the CR and its helix–helix contacts. NMR spectroscopy is a powerful technique that provides atomic resolution information on biomolecular structure and contacts. The 2D NMR spectrum is the fingerprint of a protein and provides direct information regarding the order/disorder of the protein as well as the formation of stable and transient contacts. Using NMR as a tool, we have previously established that TDP-43 CR α-helix self-assembly can be monitored as chemical shift perturbations (CSP) in CR residues upon increasing the protein concentration in conditions where TDP-43 CTD does not readily phase separate (i.e., low salt conditions) (Fig. 5*A*, WT CTD panel, ref. 16). To access the impact of mutations that alter TDP-43 CTD phase separation, we compared the 2D NMR spectrum of the variants with that of the WT CTD at 20 μM (a monomeric reference) and 90 μM (Fig. 5*A*). Interestingly, the resonances arising from residue positions in the CR for 5M→A^{IDR} and 6F→A were nearly unperturbed compared to WT CTD at low protein concentration (20 μM), suggesting the α-helical structure of the monomeric CR is intact in these constructs. For WT CTD, we observed significant up-field ^{15}N CSP at 90 μM for the CR residues corresponding to self-interaction and enhanced helicity (16, 54). However, the CSPs for CR residues in 5M→A^{IDR} were reduced and were minimal in 6F→A compared to WT CTD (Fig. 5*B*), indicating disruption in the helix–helix assembly. Taken together, these data suggest that phenylalanine and methionine outside of the CR form contacts important in helix-mediated CTD oligomerization in the early stages of self-assembly preceding phase separation. Importantly, the substitution of these residues has no impact on CR helicity, consistent with the model that partial CR helical structure is stable and does not require contacts outside the CR.

Previously, we showed that the helix-disfavoring M337V ALS-associated mutation disrupts helix–helix assembly, as does an engineered proline mutation M337P which is incompatible with helical structure (16). This observation prompted us to test whether the methionine residues play a critical role in helix–helix interactions beyond stabilizing the helix itself. To this end, we tested the 5M→A^{CR} variant (that substitutes all five conserved region methionine positions to alanine—M322A, M323A, M336A, M337A, and M339A, see above). As expected, the two-dimensional spectral fingerprint at the CR was significantly perturbed by the substitution of the 5 methionine residues. In order to identify the CR residues, we carried out standard triple resonance NMR assignment experiments (including the HNN experiment, see *Methods*) and obtained backbone amide resonance assignments. Interestingly, substitution of all five conserved region methionine positions to alanine (5M→A^{CR}) prevented assembly of the CR region, as little to no CSPs for the CR residues were observed upon increasing concentration (Fig. 5 *A* and *B*). Therefore, these data suggest the methionine residues in the CR are important for mediating helix–helix assembly probably due to the loss of methionine side-chain contacts. To test whether the mutations disrupt helicity, we calculated the secondary structure content of the CR in 5M→A^{CR}. Secondary structure analysis was performed by comparing the experimental C_α and C_β chemical shifts with their predicted random coil shifts, $\Delta\delta C_\alpha - \Delta\delta C_\beta$ (55, 56), as we did previously for TDP-43 CTD WT and helix-enhancing mutants (16, 19). Surprisingly, our NMR data analysis revealed a significant population of helical structures based on residual ^{13}C chemical shifts that are very similar to WT CTD. As a control, these values are also significantly higher than those in the helix-disrupting A326P variant (16) (Fig. 5*C*). However, it should be pointed out that the secondary structure propensity of alanine residues at 322 and 323 positions are even more positive than those for methionine at these positions in WT CTD, possibly due to the higher helicity for polyalanine sequences (52). Still, the helicity was slightly smaller in other locations compared to WT CR, suggesting that these conserved methionines also form intramolecular contacts to stabilize the helix in TDP-43 CTD. Taken together, these data show that methionines are important for intermolecular contacts that mediate helical assembly and stabilize the helix.

Discussion

We adopted a hybrid simulation-based strategy coupled with in vitro experiments to identify the relative contribution of prevalent hydrophobic residues which modulate the phase separation of TDP-43 CTD. Our results indicate that the substitution of phenylalanine residues (6F→A) outside CR significantly reduces the phase separation of CTD. Along similar lines, F→S substitution within the CTD was previously shown to disrupt phase separation in vivo for a reporter TDP-43 construct and in vitro for full-length TDP-43 (21). TDP-43 CTD contains methionine residues which are equally distributed (five each) in the CR and the flanking regions. We observed that the substitution of methionines outside the CR (5M→A^{IDR}) also weakens phase separation, while 5M→A^{CR} mutant significantly disrupts phase separation.

Further, reduced phase separation caused by removing the methionines inside the CR (5M→A^{CR}) could be alleviated with the addition of methionine residues in the region flanking the CR (5A→M^{IDR} + 5M→A^{CR}). Along similar lines, M/V→A substitutions within the methionine-rich LC domain of Pab-1 were found to modulate its phase separation through an increase in the radius of gyration and demixing temperature (57). Additionally, methionines in the FUS RGG3 domain have been shown to make contacts with the FUS SYGQ low complexity domain within a cocondensed phase (58). In sum, methionine residues, surprisingly, substantially contribute toward interactions that drive the phase separation of CTD.

It is important to consider the relative contribution of methionine towards phase separation compared to other aromatic and aliphatic residues. CG simulations and experimental data show that it has lower stabilizing contributions to phase separation than the aromatic residue—tyrosine (5M→Y^{IDR}). Substitutions of methionine with another aliphatic residue, leucine (5M→L^{IDR}), yielded minor changes in phase separation compared to WT by experiment and simulation. Likewise, 5M→S mutation in IDR1/2 is shown to increase droplet dynamics without affecting its c_{sat}, while 5M→V behaved similarly to WT for a TDP-43 reporter construct under in vivo conditions (21). Our

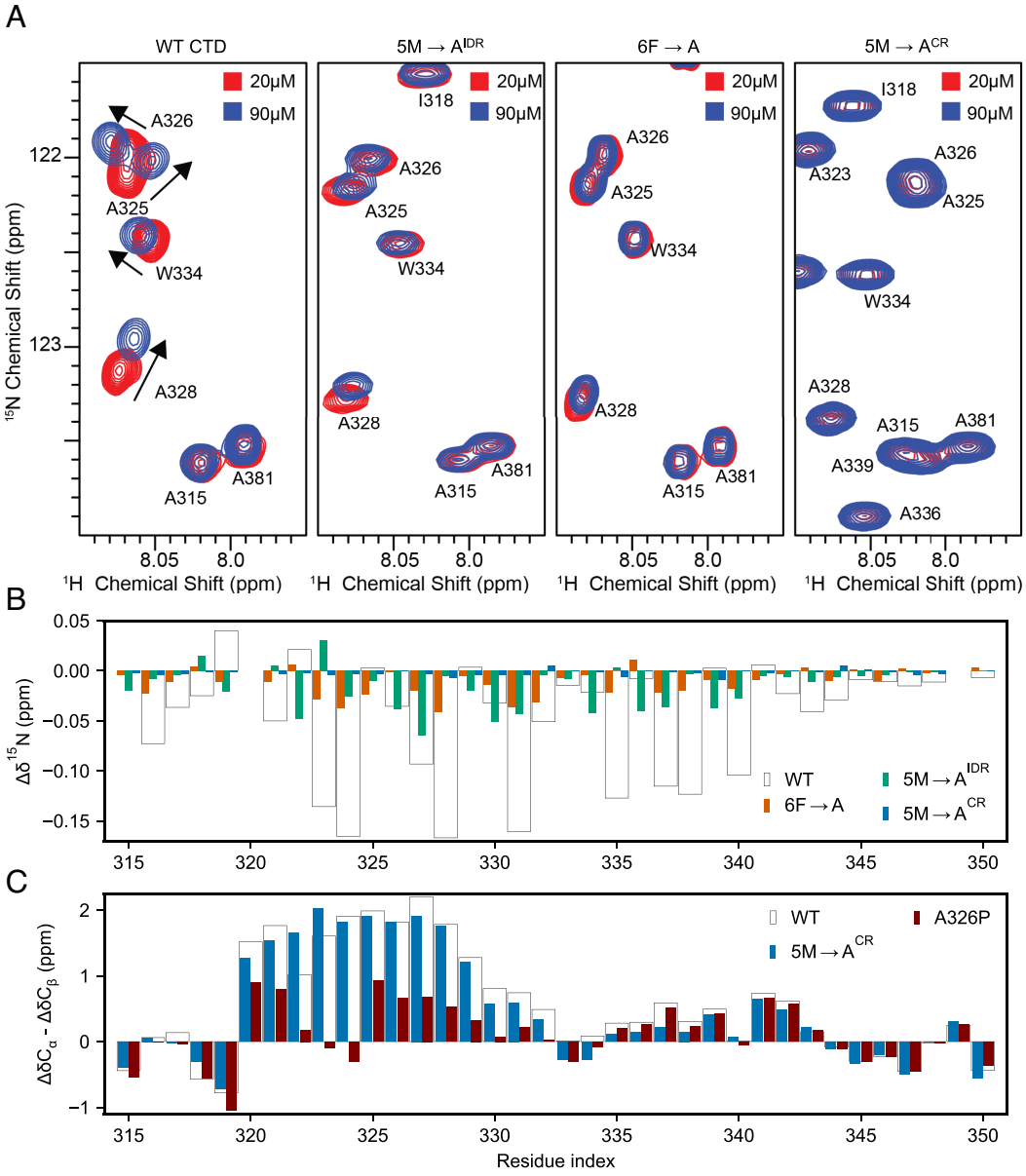

Fig. 5. Phenylalanine and methionine residues are crucial for TDP-43 self-assembly. (*A*) Overlay of ^{1}H–^{15}N HSQC spectra of the TDP-43 CTD at two concentrations 20 μM (red) and 90 μM (blue), showing chemical shift perturbations (arrows) associated with intermolecular interactions. The chemical shift deviations are minimal for 6F→A variant and reduced for 5M→A^{IDR} variant, whereas 5M→A^{CR} does not show chemical shift deviations up to 90 μM protein concentrations. The WT CTD and 6F→A spectra were recorded at 850 MHz, while the 5M→A^{IDR} and 5M→A^{CR} spectra were recorded at 600 MHz. (*B*) A comparison of ^{15}N chemical shift differences ($\Delta\delta^{15}N$) for the CR of WT CTD versus its designed variants confirms the disruption of helix–helix interactions by these variants. (*C*) Secondary shifts ($\Delta\delta C_\alpha$-$\Delta\delta C_\beta$) of 5M→A^{CR} mutant relative to WT CTD and helix-disrupting A326P show that 5M→A^{CR} conserves the helix present in WT CTD.

observations here provide direct evidence for the contribution of methionine to the thermodynamics of phase separation. Furthermore, our results suggest that other aliphatic residues except alanine may have similar contributions, expanding the molecular grammar of low-complexity domain phase separation.

Our sequence alignment analysis over 93 homologs of TDP-43 CTD (21) shows that the number of aliphatic residues (L = 2, I = 1, and M = 5) outside CR is mostly conserved and switched to another aliphatic residue (VLIM) in some homologs (e.g., L270, I383) (*SI Appendix*, Fig. S12). On the other hand, alanine, which is also aliphatic, is less conserved and tends to switch to or appear as a replacement for polar residues. Correspondingly, our in vitro experiments support the idea that alanine residues outside CR contribute less to LLPS than larger aliphatic residues. Although aliphatic residues may contribute to phase separation similarly based on their similar hydrophobicity and size, it is important to note that methionine has unique physicochemical properties that could broaden its role in phase separation (59).

An important characteristic of methionine is its ability to undergo reversible oxidation (60, 61) which allows for the regulation of protein phase separation. This was probed in detail by the recent studies from the Tu (62) and McKnight (63) laboratories wherein the methionine-rich LC domain self-association of yeast ataxin-2 was demonstrated to be controlled by reversible methionine oxidation. Similarly, phase separation of TDP-43 CTD was shown to be disrupted in vitro due to the nonspecific oxidation of methionines in the presence of H_2O_2, an oxidizing agent, and restored via enzymatic reduction of methionine oxidation (64). However, these studies do not provide direct evidence of why methionine oxidation disrupts phase separation. Our findings based

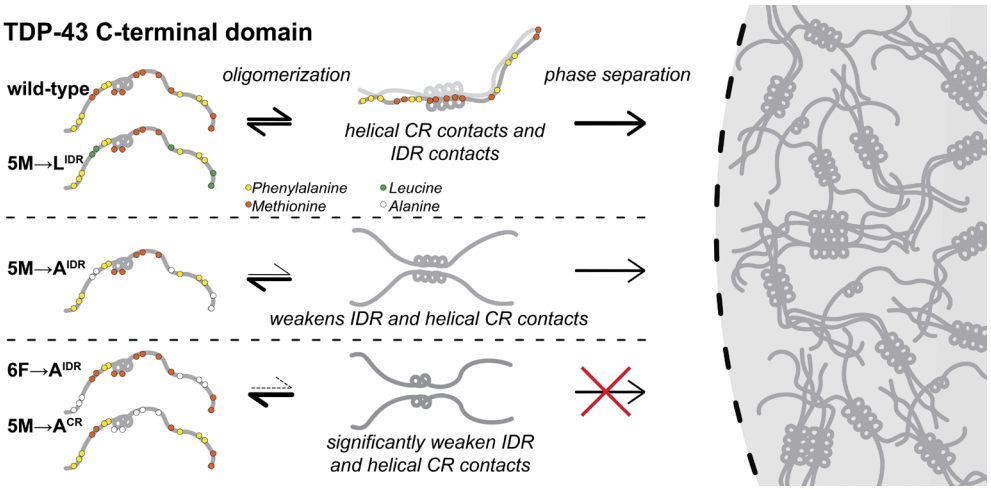

Fig. 6. LLPS of TDP-43 C-terminal domain is governed by synergistic interactions involving hydrophobic residues in both CR and flanking regions. Schematic highlighting the involvement of both phenylalanine (aromatic) and methionine (aliphatic) residues in driving the formation of the oligomeric intermediate enroute to LLPS of CTD. Both wild-type and 5M→L^{IDR} (preserves hydrophobicity of IDR1/2) variant undergo oligomerization through the formation of transient IDR contacts and site-specific CR contacts. In contrast, the loss of hydrophobicity in 5M→A^{IDR}, 6F→A^{IDR} and 5M→A^{CR} variants disrupts oligomerization and LLPS by weakening both IDR and CR contacts.

on explicit evaluation of c_{sat} for M→A variants directly attribute methionine's role in CTD phase separation.

Upon methionine composition analysis of 29 human RBP prion candidates (65), including ataxin-2, we found that one-third of those PrLDs contain at least 4% methionine (*SI Appendix*, Table S2, and Fig. S13). These observations suggest that the results reported in this study regarding the requirement of methionine residues in TDP-43 CTD phase separation could be general for other PrLDs. Interestingly, the cryo-EM structure (66) of aggregated TDP-43 from the human brain of an individual affected by ALS with FTLD has a cluster of methionine and phenylalanine residues in the core (M307, M311, F313, M322, and M323) and numerous methionine-aromatic contacts can be seen at different locations. This implies that the presence of energetically stabilizing aliphatic-aromatic contacts may promote fibrillization from the condensed phase.

Recently, it was shown that disordered regions flanking the binding interface could modulate the binding affinity between two transcriptional coactivators—CBP and NCOA, through transient hydrophobic interactions (67). Interestingly, our findings also lead us to propose a similar mode of biomolecular recognition wherein a synergy between site-specific (CR-mediated) and transient (IDR-mediated) interactions involving hydrophobic residues (phenylalanine/methionine) drive the oligomerization and subsequent phase separation of TDP-43 C-terminal domain (Fig. 6). Overall, these findings highlight the rich diversity of interaction modes which underlie protein–protein association and the formation of higher-order assemblies such as biomolecular condensates (68, 69).

Methods

Refer to *SI Appendix* for details. MD simulations were performed to predict the molecular interactions underlying the phase behavior of wild-type human TDP-43 CTD and relative changes in c_{sat} upon sequence mutations. Wild-type human CTD and its mutant variants were cloned from codon-optimized sequences into the pJ411 bacterial expression vector (N-terminal 6x-His tag), expressed in *Escherichia coli* and purified by affinity chromatography. DIC microscopy was used to qualitatively characterize the extent of phase separation of wild-type CTD and its mutant variants. To quantify phase separation in vitro, assays were conducted for protein samples with increasing salt concentration to determine c_{sat}. NMR experiments were performed to assess the impact of sequence mutations on CTD oligomerization and the helicity of the CR.

Data, Materials, and Software Availability. NMR chemical shift assignments in this paper for TDP-43 CTD WT (26823) (70), A326P (26828) (71), 6F→A (52061) (72), 5M→A^{IDR} (52062) (73), and 5M→A^{CR} (52060) (74) can be obtained online from the Biological Magnetic Resonance Database (BMRB). Plasmids generated for this project can be found at Addgene.org (deposition in process). The simulation protocols along with the URL for the appropriate codes are provided in *SI Appendix*.

ACKNOWLEDGMENTS. P.M. thanks Nina Jovic for helping with setting up PT-WTE simulations. This work was supported by NINDS and NIA R01NS116176. J.S. was supported by a Milton Safenowitz Postdoctoral Fellowship from the ALS Association and Judith and Jean Pape Adams Postdoctoral Fellowship at Brown University. Atomistic and coarse-grained simulations were conducted with the advanced computing resources provided by Texas A&M High Performance Research Computing. NMR experiments were conducted with the support of the Structural Biology Core Facility in the Division of Biology and Medicine at Brown University and with assistance from Mandar Naik.

Author affiliations: [a]Artie McFerrin Department of Chemical Engineering, Texas A&M University, College Station, TX 77843; [b]Department of Molecular Biology, Cell Biology & Biochemistry, Brown University, Providence, RI 02912; [c]Department of Chemistry, Texas A&M University, College Station, TX 77843; and [d]Interdisciplinary Graduate Program in Genetics and Genomics, Texas A&M University, College Station, TX 77843

1. B. S. Schuster *et al.*, Biomolecular condensates: Sequence determinants of phase separation, microstructural organization, enzymatic activity, and material properties. *J. Phys. Chem. B* **125**, 3441–3451 (2021).
2. S. F. Banani, H. O. Lee, A. A. Hyman, M. K. Rosen, Biomolecular condensates: Organizers of cellular biochemistry. *Nat. Rev. Mol. Cell Biol.* **18**, 285–298 (2017).
3. B. R. Sabari, A. Dall'Agnese, R. A. Young, Biomolecular condensates in the nucleus. *Trends Biochem. Sci.* **45**, 961–977 (2020).
4. A. A. Hyman, C. A. Weber, F. Julicher, Liquid-liquid phase separation in biology. *Annu. Rev. Cell Dev. Biol.* **30**, 39–58 (2014).
5. K. Rhine, V. Vidaurre, S. Myong, RNA droplets. *Annu. Rev. Biophys.* **49**, 247–265 (2020).
6. D. S. W. Protter, R. Parker, Principles and properties of stress granules. *Trends Cell Biol.* **26**, 668–679 (2016).
7. A. F. Harrison, J. Shorter, RNA-binding proteins with prion-like domains in health and disease. *Biochem. J.* **474**, 1417–1438 (2017).
8. T. Mittag, R. Parker, Multiple modes of protein-protein interactions promote RNP granule assembly. *J. Mol. Biol.* **430**, 4636–4649 (2018).
9. W. M. Babinchak, W. K. Surewicz, Liquid-liquid phase separation and its mechanistic role in pathological protein aggregation. *J. Mol. Biol.* **432**, 1910–1925 (2020).

10. T. J. Cohen, V. M. Lee, J. Q. Trojanowski, TDP-43 functions and pathogenic mechanisms implicated in TDP-43 proteinopathies. *Trends Mol. Med.* **17**, 659–667 (2011).
11. M. Neumann *et al.*, Ubiquitinated TDP-43 in frontotemporal lobar degeneration and amyotrophic lateral sclerosis. *Science* **314**, 130–133 (2006).
12. T. Afroz *et al.*, Functional and dynamic polymerization of the ALS-linked protein TDP-43 antagonizes its pathologic aggregation. *Nat. Commun.* **8**, 45 (2017).
13. A. Wang *et al.*, A single N-terminal phosphomimic disrupts TDP-43 polymerization, phase separation, and RNA splicing. *EMBO J.* **37**, e97452 (2018).
14. P. J. Lukavsky *et al.*, Molecular basis of UG-rich RNA recognition by the human splicing factor TDP-43. *Nat. Struct. Mol. Biol.* **20**, 1443–1449 (2013).
15. L. Z. Lim, Y. Y. Wei, Y. M. Lu, J. X. Song, ALS-causing mutations significantly perturb the self-assembly and interaction with nucleic acid of the intrinsically disordered prion-like domain of TDP-43. *Plos Biol.* **14**, e1002338 (2016).
16. A. E. Conicella, G. H. Zerze, J. Mittal, N. L. Fawzi, ALS Mutations disrupt phase separation mediated by alpha-helical structure in the TDP-43 low-complexity C-terminal domain. *Structure* **24**, 1537–1549 (2016).
17. H. R. Li *et al.*, The physical forces mediating self-association and phase-separation in the C-terminal domain of TDP-43. *Biochim. Biophys. Acta Proteins Proteom.* **1866**, 214–223 (2018).
18. H. B. Schmidt, R. Rohatgi, In vivo formation of vacuolated multi-phase compartments lacking membranes. *Cell Rep.* **16**, 1228–1236 (2016).
19. A. E. Conicella *et al.*, TDP-43 alpha-helical structure tunes liquid-liquid phase separation and function. *Proc. Natl. Acad. Sci. U.S.A.* **117**, 5883–5894 (2020).
20. H. R. Li, W. C. Chiang, P. C. Chou, W. J. Wang, J. R. Huang, TAR DNA-binding protein 43 (TDP-43) liquid-liquid phase separation is mediated by just a few aromatic residues. *J. Biol. Chem.* **293**, 6090–6098 (2018).
21. H. B. Schmidt, A. Barreau, R. Rohatgi, Phase separation-deficient TDP43 remains functional in splicing. *Nat. Commun.* **10**, 4890 (2019).
22. D. Pantoja-Uceda *et al.*, Phe-Gly motifs drive fibrillization of TDP-43's prion-like domain condensates. *Plos Biol.* **19**, e3001198 (2021).
23. J. Wang *et al.*, A molecular grammar governing the driving forces for phase separation of prion-like RNA binding proteins. *Cell* **174**, 688–699.e16 (2018).
24. E. W. Martin *et al.*, Valence and patterning of aromatic residues determine the phase behavior of prion-like domains. *Science* **367**, 694–699 (2020).
25. A. Bremer *et al.*, Deciphering how naturally occurring sequence features impact the phase behaviours of disordered prion-like domains. *Nat. Chem.* **14**, 196–207 (2022).
26. B. S. Schuster *et al.*, Identifying sequence perturbations to an intrinsically disordered protein that determine its phase-separation behavior. *Proc. Natl. Acad. Sci. U.S.A.* **117**, 11421–11431 (2020).
27. A. Barducci, J. Pfaendtner, M. Bonomi, "Tackling sampling challenges in biomolecular simulations" in *Molecular Modeling of Proteins*, A. Kukol, Ed. (Springer, New York, NY, 2015), pp. 151–171. 10.1007/978-1-4939-1465-4_8.
28. J. E. Shea, R. B. Best, J. Mittal, Physics-based computational and theoretical approaches to intrinsically disordered proteins. *Curr. Opin. Struct. Biol.* **67**, 219–225 (2021).
29. P. Robustelli, S. Piana, D. E. Shaw, Developing a molecular dynamics force field for both folded and disordered protein states. *Proc. Natl. Acad. Sci. U.S.A.* **115**, E4758–E4766 (2018).
30. K. Lindorff-Larsen, N. Trbovic, P. Maragakis, S. Piana, D. E. Shaw, Structure and dynamics of an unfolded protein examined by molecular dynamics simulation. *J. Am. Chem. Soc.* **134**, 3787–3791 (2012).
31. M. Bernetti *et al.*, Structural and kinetic characterization of the intrinsically disordered protein SeV NTAIL Through enhanced sampling simulations. *J. Phys. Chem. B* **121**, 9572–9582 (2017).
32. U. R. Shrestha *et al.*, Generation of the configurational ensemble of an intrinsically disordered protein from unbiased molecular dynamics simulation. *Proc. Natl. Acad. Sci. U.S.A.* **116**, 20446–20452 (2019).
33. G. H. Zerze, R. B. Best, J. Mittal, Sequence- and temperature-dependent properties of unfolded and disordered proteins from atomistic simulations. *J. Phys. Chem. B* **119**, 14622–14630 (2015).
34. N. Sibille, P. Bernado, Structural characterization of intrinsically disordered proteins by the combined use of NMR and SAXS. *Biochem. Soc. Trans.* **40**, 955–962 (2012).
35. S. J. LeBlanc, P. Kulkarni, K. R. Weninger, Single molecule FRET: A powerful tool to study intrinsically disordered proteins. *Biomolecules* **8**, 140 (2018), 10.3390/biom8040140.
36. G. L. Dignon, W. Zheng, Y. C. Kim, R. B. Best, J. Mittal, Sequence determinants of protein phase behavior from a coarse-grained model. *PLoS Comput. Biol.* **14**, e1005941 (2018).
37. R. M. Regy, J. Thompson, Y. C. Kim, J. Mittal, Improved coarse-grained model for studying sequence dependent phase separation of disordered proteins. *Protein Sci.* **30**, 1371–1379 (2021).
38. G. L. Dignon, W. Zheng, R. B. Best, Y. C. Kim, J. Mittal, Relation between single-molecule properties and phase behavior of intrinsically disordered proteins. *Proc. Natl. Acad. Sci. U.S.A.* **115**, 9929–9934 (2018).
39. Y. H. Lin, H. S. Chan, Phase separation and single-chain compactness of charged disordered proteins are strongly correlated. *Biophys. J.* **112**, 2043–2046 (2017).
40. A. C. Murthy *et al.*, Molecular interactions underlying liquid-liquid phase separation of the FUS low-complexity domain. *Nat. Struct. Mol. Biol.* **26**, 637–648 (2019).
41. V. H. Ryan *et al.*, Mechanistic view of hnRNPA2 low-complexity domain structure, interactions, and phase separation altered by mutation and arginine methylation. *Mol. Cell* **69**, 465–479 e467 (2018).
42. W. S. Tang, N. L. Fawzi, J. Mittal, Refining all-atom protein force fields for polar-rich, prion-like, low-complexity intrinsically disordered proteins. *J. Phys. Chem. B* **124**, 9505–9512 (2020).
43. R. B. Best, W. Zheng, J. Mittal, Balanced protein-water interactions improve properties of disordered proteins and non-specific protein association. *J. Chem. Theory Comput.* **10**, 5113–5124 (2014).
44. M. Deighan, M. Bonomi, J. Pfaendtner, Efficient simulation of explicitly solvated proteins in the well-tempered ensemble. *J. Chem. Theory Comput.* **8**, 2189–2192 (2012).
45. Y. Shen, A. Bax, SPARTA+: A modest improvement in empirical NMR chemical shift prediction by means of an artificial neural network *J. Biomol. NMR* **48**, 13–22 (2010).
46. W. Kabsch, C. Sander, Dictionary of protein secondary structure: Pattern recognition of hydrogen-bonded and geometrical features. *Biopolymers* **22**, 2577–2637 (1983).
47. C. Camilloni, A. De Simone, W. F. Vranken, M. Vendruscolo, Determination of secondary structure populations in disordered states of proteins using nuclear magnetic resonance chemical shifts. *Biochemistry* **51**, 2224–2231 (2012).
48. I. M. Zeron, J. L. F. Abascal, C. Vega, A force field of Li(+), Na(+), K(+), Mg(2+), Ca(2+), Cl(-), and SO4 (2-) in aqueous solution based on the TIP4P/2005 water model and scaled charges for the ions *J. Chem. Phys.* **151**, 134504 (2019).
49. R. M. Vernon *et al.*, Pi-Pi contacts are an overlooked protein feature relevant to phase separation. *Elife* **7**, e31486 (2018).
50. D. W. Urry *et al.*, Hydrophobicity scale for proteins based on inverse temperature transitions. *Biopolymers* **32**, 1243–1250 (1992).
51. T. D. Nguyen, C. L. Phillips, J. A. Anderson, S. C. Glotzer, Rigid body constraints realized in massively-parallel molecular dynamics on graphics processing units. *Comput. Phys. Commun.* **182**, 2307–2313 (2011).
52. R. J. Moreau *et al.*, Context-independent, temperature-dependent helical propensities for amino acid residues. *J. Am. Chem. Soc.* **131**, 13107–13116 (2009).
53. I. R. Mackenzie *et al.*, TIA1 Mutations in amyotrophic lateral sclerosis and frontotemporal dementia promote phase separation and alter stress granule dynamics. *Neuron* **95**, 808–816.e9 (2017).
54. Y. J. Wang, O. Jardetzky, Probability-based protein secondary structure identification using combined NMR chemical-shift data. *Protein Sci.* **11**, 852–861 (2002).
55. M. Kjaergaard, F. M. Poulsen, Sequence correction of random coil chemical shifts: Correlation between neighbor correction factors and changes in the Ramachandran distribution. *J. Biomol. NMR* **50**, 157–165 (2011).
56. M. Kjaergaard, S. Brander, F. M. Poulsen, Random coil chemical shift for intrinsically disordered proteins: Effects of temperature and pH. *J. Biomol. NMR* **49**, 139–149 (2011).
57. J. A. Riback *et al.*, Stress-triggered phase separation is an adaptive, evolutionarily tuned response. *Cell* **168**, 1028–1040.e19 (2017).
58. A. C. Murthy *et al.*, Molecular interactions contributing to FUS SYGQ LC-RGG phase separation and co-partitioning with RNA polymerase II heptads. *Nat. Struct. Mol. Biol.* **28**, 923–935 (2021).
59. J. C. Aledo, Methionine in proteins: The Cinderella of the proteinogenic amino acids. *Protein Sci.* **28**, 1785–1796 (2019).
60. J. Moskovitz, B. S. Berlett, J. M. Poston, E. R. Stadtman, The yeast peptide methionine sulfoxide reductase functions as an antioxidant in vivo. *Proc. Natl. Acad. Sci. U.S.A.* **94**, 9585–9589 (1997).
61. C. Achilli, A. Ciana, G. Minetti, The discovery of methionine sulfoxide reductase enzymes: An historical account and future perspectives. *Biofactors* **41**, 135–152 (2015).
62. Y. S. Yang *et al.*, Yeast Ataxin-2 forms an intracellular condensate required for the inhibition of TORC1 signaling during respiratory growth. *Cell* **177**, 697–710.e17 (2019).
63. M. Kato *et al.*, Redox state controls phase separation of the yeast Ataxin-2 protein via reversible oxidation of its methionine-rich low-complexity domain. *Cell* **177**, 711–721 e718 (2019).
64. Y. Lin *et al.*, Redox-mediated regulation of an evolutionarily conserved cross-beta structure formed by the TDP43 low complexity domain. *Proc. Natl. Acad. Sci. U.S.A.* **117**, 28727–28734 (2020).
65. O. D. King, A. D. Gitler, J. Shorter, The tip of the iceberg: RNA-binding proteins with prion-like domains in neurodegenerative disease. *Brain Res.* **1462**, 61–80 (2012).
66. D. Arseni *et al.*, Structure of pathological TDP-43 filaments from ALS with FTLD. *Nature* **601**, 139–143 (2022).
67. E. Karlsson *et al.*, Disordered regions flanking the binding interface modulate affinity between CBP and NCOA. *J. Mol. Biol.* **434**, 167643 (2022).
68. G. L. Dignon, R. B. Best, J. Mittal, Biomolecular phase separation: From molecular driving forces to macroscopic properties. *Annu. Rev. Phys. Chem.* **71**, 53–75 (2020).
69. P. Mohanty *et al.*, Principles governing the phase separation of multidomain proteins. *Biochemistry* **61**, 2443–2455 (2022).
70. A. Conicella, N. L. Fawzi, Backbone 1H, 13C, and 15N Chemical Shift Assignments, HNHA scalar coupling, and 15N backbone relaxation data for TDP-43 C-terminal domain wild type. Biological Magnetic Resonance Data Bank (BMRB). https://bmrb.io/data_library/summary/?bmrbId=26823. Accessed 17 October 2022.
71. A. Conicella, N. L. Fawzi, Backbone 1H, 13C, and 15N Chemical Shift Assignments for TDP-43 C-terminal domain engineered variant A326P. Biological Magnetic Resonance Data Bank (BMRB). https://bmrb.io/data_library/summary/index.php?bmrbId=26828. Accessed 17 October 2022.
72. J. Shenoy, N. L. Fawzi, Backbone 1H and 15N Chemical Shift Assignments for the region 310–350 of TDP-43 C-terminal domain engineered variant 6F to A. Biological Magnetic Resonance Data Bank (BMRB). https://bmrb.io/data_library/summary/index.php?bmrbId=52061. Deposited 30 July 2023.
73. J. Shenoy, N. L. Fawzi, Backbone 1H and 15N Chemical Shift Assignments for the region 310–350 of TDP-43 C-terminal domain engineered variant 5M to A outside CR. Biological Magnetic Resonance Data Bank (BMRB). https://bmrb.io/data_library/summary/index.php?bmrbId=52062. Deposited 30 July 2023.
74. J. Shenoy, N. L. Fawzi, Backbone 1H, 13C, and 15N Chemical Shift Assignments for the region 310–350 of TDP-43 C-terminal domain engineered variant 5M to A inside CR. Biological Magnetic Resonance Data Bank (BMRB). https://bmrb.io/data_library/summary/index.php?bmrbId=52060. Deposited 29 July 2023.